

EVIDENCE FOR INTERMEDIATE BLR OF REVERBERATION-MAPPED AGN PG 0052+251

XUE-GUANG ZHANG^{1,2}

Draft version August 16, 2011

ABSTRACT

In this manuscript, we study properties of BLR of well-known reverberation-mapped AGN, in order to find reliable evidence for intermediate BLR. We firstly check properties of mapped AGN collected from literature in plane of $\sigma_{\text{H}\beta}^2/\sigma_{\text{H}\alpha}^2$ vs $R_{\text{BLR}}^{\text{H}\alpha}/R_{\text{BLR}}^{\text{H}\beta}$. Commonly, virial BH masses based on observed broad H α and H β should be coincident. However, among the mapped objects, PG0052 and NGC4253 are two apparent outliers in the plane of $\sigma_{\text{H}\beta}^2/\sigma_{\text{H}\alpha}^2$ vs $R_{\text{BLR}}^{\text{H}\alpha}/R_{\text{BLR}}^{\text{H}\beta}$, which indicate BLRs of PG0052 and NGC4253 have some special characters. Then based on the 55 public spectra of PG0052, BLR of PG0052 is been carefully studied in detail. We find that line width ratio of total observed broad H α to total observed broad H β is ~ 0.7 , which is much smaller than theoretical/observational value of ~ 0.9 . Furthermore, flux ratio of total broad H α to total broad H β is about 6.8 (Balmer Decrement), which is not one reasonable value for BLUE quasar PG 0052+251. Moreover, properties of line cores based on PCA technique confirm there is one inner broad component and one seriously obscured intermediate broad component in BLR of PG0052. If the seriously obscured intermediate BLR was accepted, properties of PG0052 in the plane of $\sigma_{\text{H}\beta}^2/\sigma_{\text{H}\alpha}^2$ vs $R_{\text{BLR}}^{\text{H}\alpha}/R_{\text{BLR}}^{\text{H}\beta}$ could be well reproduced, which indicates that the intermediate BLR actually is well appropriate to mapped quasar PG 0052+251. Finally, the large distance between inner component of BLR and intermediate component of BLR based on CCF results rejects the possibility that the intermediate component is probably extended part of inner component of BLR.

Subject headings: Galaxies:Active – Galaxies:nuclei – Galaxies:quasars:Emission lines – Galaxies: Individual: PG 0052+251.

1. INTRODUCTION

Through strong broad emission lines coming from Broad Line Regions (BLR) of Active Galactic Nuclei (AGN), properties of BLR of AGN which can not be directly resolved by current observational technique and instruments have been understood deeper and deeper (see reviews of Sulentic et al. 2000; Gaskell 2010; Krause et al. 2011; Denney et al. 2010; Netzer & Marziani 2010; Sluse et al. 2011; Pancoast et al. 2011 etc., and references therein). Based on properties of BLR of AGN (especially virialized emission line clouds in BLR, Gaskell 1988; Wandel et al. 1999; Peterson & Wandel 1999; Osterbrock & Mathews 1986; Denney et al. 2009; Gaskell 2009), the most convenient method to estimate virial BH masses of broad line AGN is proposed (Vestergaard 2002; Onken et al. 2004; Peterson et al. 2004; Peterson 2010; Peterson & Bentz 2006; Collin et al. 2006; Kelly & Bechtold 2007)

$$M_{\text{BH}} \propto V^2 \times R_{\text{BLR}} \quad (1)$$

where V represents probable rotating velocity of emission line clouds in BLR (line width of broad emission line), R_{BLR} means distance between BLR and central black hole of AGN (size of BLR) which can be measured by time lag between broad line emission and continuum emission from long-period observed spectra (Kaspi et al. 2000; Peterson et al. 2004; Bentz et al.

2006, 2009; Denney et al. 2010) based on the reverberation mapping technique (Blandford & McKee 1982; Peterson 1993). There are so far more than 40 nearby broad line objects, of which R_{BLR} and virial BH masses have been determined (Peterson et al. 2004; Denney et al. 2010; Kaspi et al. 2005; Bentz et al. 2009, 2010; Barth et al. 2011). Then one empirical relation has been found for R_{BLR} , $R_{\text{BLR}} \propto L_{5100}^{0.5} \propto L_{\text{line}}^{0.5}$, where L_{5100} means AGN continuum luminosity at 5100Å and L_{line} represents broad line luminosity (Kaspi et al. 2005; Denney et al. 2010; Bentz et al. 2009; Wang & Zhang 2003; Greene et al. 2010), and virial BH masses can be simply and conveniently estimated from single epoch spectra of broad line AGN by line width and continuum luminosity (or broad line luminosity) (Vestergaard 2002; McLure & Dunlop 2004; Sulentic et al. 2000; Netzer & Marziani 2010; Sulentic et al. 2006, 2007; Shen et al. 2008; Rafiee & Hall 2011; Netzer & Marziani 2010; Kelly & Bechtold 2007; Greene & Ho 2005; Denney et al. 2009a)

$$M_{\text{BH}} \propto V^2 \times L_{5100}^{0.5} \propto V^2 \times L_{\text{line}}^{0.5} \quad (2)$$

It is clear that from single epoch spectra of broad line AGN, virial BH masses based on different broad emission lines should be coincident. However, some conflicting results have been reported. Kelly & Bechtold (2007) have found that virial BH masses based on broad lines in UV band and broad lines in optical band are coincident well (some simple and more recent results can also be found in Rafiee & Hall 2011). However, Sulentic et al. (2007) have shown that UV broad line CIV $\lambda 1545\text{\AA}$ is a poor virial estimator. Recently, Assef et al. (2010) have

¹ Purple Mountain Observatory, Chinese Academy of Sciences, 2 Beijing Xi Lu, Nanjing, Jiangsu, 210008, P. R. China; xgzhang@pmo.ac.cn

² Department of Physics and Astronomy, Texas A&M University, College Station, TX 77843-4242, USA

found the opposite that virial BH mass estimates Based on CIV λ 1545Å are consistent with those based on the balmer lines. Different virial BH masses based on different broad emission lines probably provide some kindly deep information of structures of BLR of AGN. In this manuscript, to study properties of virial BH masses on different broad emission lines for reverberation-mapped AGN is our main objective. In order to find more reliable results, parameters based on the reverberation-mapped AGN rather than AGN with single epoch spectra should be firstly considered. For recent reported reverberation-mapped AGN, sizes of BLR are based on long-period varied broad line emission lines in optical band, especially balmer lines. Thus, in the manuscript, we mainly consider the properties of balmer lines ($H\alpha$ and $H\beta$) of reverberation mapped AGN.

Besides the reverberation mapping technique and virialization method for virial BH masses, there are some references which study properties of emission lines regions for broad optical balmer lines. Korista & Goad (2004) have shown that after consideration of luminosity dependent responsivities, theoretically estimated size of BLR based on $H\alpha$ should be 20% larger than size of BLR based on $H\beta$, and corresponding line width of $H\beta$ should be some larger than that of $H\alpha$. The theoretical results can be confirmed by observational results shown in Bentz et al. (2010) (size of BLR on $H\alpha$ is some larger than size of BLR on $H\beta$) for mapped objects and in Greene & Ho (2005) (line width of broad $H\beta$ is some larger than line width of broad $H\alpha$) for pure quasars. Furthermore, one called two-component model of BLR has been proposed (Popovic 2007; Bon et al. 2009; Zhu et al. 2009; Hu et al. 2008): one inner region for broad wings and one intermediate region for cores, in order to explain complexed broad lines of AGN. Although estimated (or measured) parameters (line width and size of BLR) of $H\alpha$ and $H\beta$ are some different to some extent, estimated virial BH masses based on $H\alpha$ and $H\beta$ should be coincident, such as the shown confirmed results in Greene & Ho (2005) for pure quasars.

It is interesting to check the virial BH masses based on $H\alpha$ and $H\beta$ for reported reverberation mapped AGN. In the manuscript, we will find that there are some mapped AGN, virial BH masses based on $H\alpha$ are much different from BH masses on $H\beta$, which will indicate some special information for structure of emission line regions for balmer lines. This manuscript is organized as follows. Section 2 shows the results based on parameters (measured line width and size of BLR based on long-period variations of line emission and continuum emission) of reported reverberation mapped AGN. Section 3 gives the detailed results for blue quasar PG 0052+251 with much different virial BH masses on $H\alpha$ and on $H\beta$. Section 4 shows the discussion and conclusion. In this manuscript, the cosmological parameters $H_0 = 70\text{km} \cdot \text{s}^{-1}\text{Mpc}^{-1}$, $\Omega_\Lambda = 0.7$ and $\Omega_m = 0.3$ have been adopted here.

2. VIRIAL BH MASSES ON BALMER LINES FOR MAPPED AGN

As shown in Introduction, we try to check virial BH masses on $H\alpha$ and $H\beta$ for mapped AGN. The reported mapped AGN are mainly included in two research groups, AGNWATCH

group (public data of 10 AGN can be found in <http://www.astronomy.ohio-state.edu/~agnwatch/>) and research group in Wise Observatory in Tel Aviv University (public data of 17 PG quasars can be found in <http://wise-obs.tau.ac.il/~shai/PG/>, Kaspi et al. 2000). Corresponding references about observational techniques and instruments for the two groups can be found in the two websites above.

Before proceeding further, we roughly check results reported in the literature (especially Kaspi et al. 2000, 2005; Peterson et al. 2004; Bentz et al. 2010) for all the 43 reverberation mapped AGN, of which observation data are public or unpublic. Here we mainly compare properties of broad $H\alpha$ and broad $H\beta$ (the two most strongest broad emission lines in optical band of AGN), including line widths (second moment rather than FWHM, which is the best approximation of V in Equation 1 as supposed by Peterson et al. 2004) and sizes of BLR (measured time lag between line emission and continuum emission, not the calculated value from empirical relation of $R \propto L^{0.5}$) based on $H\alpha$ ($R_{\text{BLR}}^{\text{H}\alpha}$) and on $H\beta$ ($R_{\text{BLR}}^{\text{H}\beta}$), which are collected and listed in Table 1. Here, only objects with reliable parameters (line width and size of BLR), $P > 1.5 \times P_{\text{err}}$ (where P means measured parameter, P_{err} represents corresponding uncertainty for the parameter) are collected from the literature. Based on the simple criterion, some reverberation-mapped objects should be rejected. For example NGC3227, its size of BLR based on $H\beta$ is $R_{\text{BLR}}^{\text{H}\beta} \sim 8.2^{+5.1}_{-8.4}\text{light} - \text{days}$, uncertainty of 8.4 is larger than measured value 8.2, thus NGC3227 is rejected. We also should note that the famous reverberation-mapped object NGC5548 is rejected due to the following reasons. On the one hand, in Peterson et al. (2004), line width of broad $H\alpha$ is not reliable due to larger uncertainty. On the other hand, we can find that size of BLR are similar, but line width of broad $H\beta$ (both second moment and FWHM) are much different in Peterson et al. (2004) from those shown in Bentz et al. (2010), $\sigma_{\text{H}\beta} \sim 2000\text{km/s}$ and $\text{FWHM}(\text{H}\beta) \sim 5800\text{km/s}$ in Peterson et al. (2004), $\sigma_{\text{H}\beta} \sim 4200\text{km/s}$ and $\text{FWHM}(\text{H}\beta) \sim 12000\text{km/s}$ in Bentz et al. (2010). Thus, NGC 5548 is not included in our parent sample listed in Table 1. Furthermore, there is another object, PG0844, we should note. For PG0844, there are reliable parameters of line width and size of BLR for broad $H\alpha$ and broad $H\beta$ in Kaspi et al. (2000), however, there is no reliable size of BLR based on $H\beta$ in Peterson et al. (2004). Thus PG 0844 is also rejected. Eventually, there are 16 objects listed in Table 1, 9 objects have public spectra (7 PG quasars observed by Wise Observatory and 2 objects included in AGNWATCH project), and the other 7 objects have no public spectra. Furthermore, we should note listed values of parameters in Table 1 are values from more recent literature. For example, values for PG0052 can be found in Kaspi et al. (2000) and in Peterson et al. (2004). Then the listed values for PG0052 are collected from Peterson et al. (2004).

As shown in introduction, it is clear that there is one strong correlation for mapped AGN based on virial BH

masses

$$\sigma_{H\alpha}^2 \times R_{BLR}^{H\alpha} = \sigma_{H\beta}^2 \times R_{BLR}^{H\beta} \quad (3)$$

$$\left(\frac{\sigma_{H\alpha}}{\sigma_{H\beta}}\right)^2 = \frac{R_{BLR}^{H\beta}}{R_{BLR}^{H\alpha}}$$

In this section, we will check the correlation for the selected mapped AGN. Figure 1 shows the correlation between line width ratio of broad H β to broad H α ($\sigma_{H\beta}^2/\sigma_{H\alpha}^2$) and size ratio of $R_{BLR}^{H\alpha}$ to $R_{BLR}^{H\beta}$ for the 16 reverberation-mapped objects listed in Table 1. For all the 16 objects, the Spearman Rank correlation coefficient for the correlation is about 0.4 with $P_{null} \sim 14\%$ (two-sided significance of deviation from zero), which indicates there is one rough positive correlation. In the figure, we also show the corresponding 99% confidence bands for the linear correlation $\sigma_{H\beta}^2/\sigma_{H\alpha}^2 = R_{BLR}^{H\alpha}/R_{BLR}^{H\beta}$. Based on the results in Figure 1, there are probable 2 outliers, PG0052 and NGC4253, which are deviating from the linear correlation supported by virialization method. After the two outliers are rejected, the re-calculated Spearman Rank correlation coefficient is about 0.9 with $P_{null} \sim 4 \times 10^{-5}$.

Based on the results shown in Figure 1, the much different virial BH masses based on H α and H β should indicate that there are some unique characters for broad balmer emission line regions. To find and study the character is the main objective of our following section. For the two outliers, only PG0052 have public observed spectra which can be downloaded from <http://wise-obs.tau.ac.il/~shai/PG/>. This, in the following section, we will mainly study the properties of reverberation mapped AGN PG0052, and try to find some special characters of broad balmer line regions of PG0052.

3. MAIN RESULTS FOR PG0052

In this paper, all the observational data and spectra of PG 0052+251 are collected from Kaspi et al. (2000) (<http://wise-obs.tau.ac.il/~shai/PG/>). The detailed description about the data and spectra can be found in Kaspi et al. (2000). Here, we do not describe instruments and observational techniques any more. There are 56 spectra from 4000Å to 8000Å with dispersion of $\sim 3.8\text{\AA}/\text{pixel}$ and spectral resolution about $\sim 10\text{\AA}$ observed from 16th Oct. 1991 to 27th Sep. 1998 for PG 0052+251. However, there is one spectrum with many bad pixels around H α , thus only 55 spectra are considered. The collected spectra from the website above have been binned into 1\AA per pixel and been padded from 3000Å to 9000Å as shown in the website. We mainly consider the data and spectra as follows.

3.1. Properties of Mean Spectrum

Mean spectrum of PG 0052+251 can be created by PCA (Principal Components Analysis or Karhunen-Loeve Transform method,) technique applied for observed noisy spectra. PCA technique is a mathematical procedure that uses an orthogonal transformation to convert a set of observations of possibly correlated variables into a set of values of uncorrelated variables called principal components. Certainly, mean subtraction (or mean centering) is necessary for performing

PCA to ensure that the first principal component describes the direction of maximum variance. However, if mean subtraction is not performed, the first eigencomponent through PCA technique commonly represents the mean spectrum of noisy spectra. Here, the convenient and public IDL PCA program 'pca_solve.pro' written by D. Schlegel in Princeton University is used, which is included in SDSS software package of IDLSPEC2D (<http://spectro.princeton.edu/>).

Figure 2 shows the mean spectrum of PG 0052+251 with relative flux density $flux(5100\text{\AA}) = 1$. Furthermore, the mean spectrum of PG 0052+251 created by Kaspi et al. (2000) is also shown in our Figure 2, which is the same as our mean spectrum created by PCA method. Then balmer emission lines are fitted by simple gaussian functions through Levenberg-Marquardt least-squares minimization method. The best fitted results are also shown in Figure 2. Emission lines around H β can be best fitted by one broad gaussian function for broad H β and three narrow gaussian functions for narrow H β and [O III] $\lambda 4959, 5007\text{\AA}$ doublet. Here when [O III]doublet is fitted, we require that [O III] $\lambda 4959, 5007\text{\AA}$ have the same line width in unit of km/s, and flux ratio of [O III] $\lambda 4959\text{\AA}$ to [O III] $\lambda 5007\text{\AA}$ is theoretical value 0.33 (Dimitrijevic et al. 2007). Emission lines around H α can be fitted by one broad gaussian function. Here we do not consider narrow emission lines around H α in the mean spectrum, due to much weak [O I] $\lambda 6300, 6363\text{\AA}$, [N II] $\lambda 6548, 6583\text{\AA}$ and [S II] $\lambda 6716, 6731\text{\AA}$ doublets. Furthermore, we should note that features of atmospheric A band near 7620\AA in observed frame can be detected, which are marked in Figure 2 and in the following Figure 4 by symbol \oplus . Here, we simply discuss effects of the features on measured line parameters. Line parameters around H α are firstly measured without any consideration of effects of the features (functions are applied to total observed line profile), and then re-measured with consideration of effects of the features (functions are applied to observed line profile with features of atmospheric A band rejected). Measured line parameters due to the two different procedures are similar. Thus, in the following part, effects of features of atmospheric A band near 7620\AA are totally ignored. The measured line parameters of broad H α and broad H β in mean spectrum are listed in Table 2.

Based on the line parameters listed in Table 2, it is clear that line width (second moment) of broad H β ($\sigma_{H\beta} \sim 38\text{\AA} \sim 2370\text{km/s}$) is much different from line width of broad H α ($\sigma_{H\alpha} \sim 37\text{\AA} \sim 1700\text{km/s}$), which is much different from the results shown in Greene & Ho (2005) and in Korista & Goad (2004) ($\sigma_{H\beta}/\sigma_{H\alpha} \sim 1.06 - 1.1$). The results indicate that broad balmer line regions of PG0052 probably have some special characters which are some different from common quasars. In other words, single broad gaussian function applied to fit broad H α and H β is not so good. Thus, we consider broad balmer emission lines by a different method as follows.

3.2. Properties of Line Cores

In order to more clearly show properties of broad balmer emission lines, PCA technique is applied again as what have been done in Brotherton et al. (1994) and

in Francis et al. (1992). Before to study properties of line cores, the commonly accepted step of mean subtraction (or mean centering) is firstly performed. Then after the PCA technique applied to the spectra with zero mean, the first principal component represents emission line cores (Brotherton et al. 1994; Francis et al. 1992). Figure 3 shows emission line cores around $H\beta$ and $H\alpha$. In the figure, line profile of $H\beta$ with flux density scaled by 3 (intrinsic flux ratio of $H\alpha$ to $H\beta$ for blue quasar) is directly compared with line profile of $H\alpha$ in the first principal component. Based on the results shown in Figure 3, it is clear that the line cores of $H\beta$ and $H\alpha$ are much different, there is one apparent broad component in $H\alpha$ but no broad component in $H\beta$ in the first principal component. The results indicate besides the similar inner broad component as that of observed broad $H\beta$, there is one other intermediate broad component in $H\alpha$ but no intermediate broad component in $H\beta$ (one seriously obscured intermediate component for balmer lines). Moreover, we should note that there are narrow lines around $H\beta$ in the first principal component shown in Figure 3, which is due to much extended component of $[OIII]\lambda 4959, 5007\text{\AA}$. Similar narrow lines can also be found in rms spectrum of PG 0844 shown in Figure 2 in Kaspi et al. (2000). Those narrow lines can not affect our results about line cores of $H\alpha$ and $H\beta$.

Thus, broad $H\alpha$ is fitted again by two gaussian functions, one broad gaussian function with similar line width as that of broad $H\beta$ and one intermediate broad gaussian function, through Levenberg-Marquardt least-squares minimization method. The two components are also shown in bottom-right panel in Figure 2. Parameters of the two components of $H\alpha$ are also listed in Table 2. The line width (second moment) of intermediate broad component of $H\alpha$ is about 1100km/s which is much larger than the line width (second moment) of narrow $[OIII]\lambda 5007$ ($\sigma([OIII]) \sim 6.6\text{\AA} = 395\text{km/s}$). Based on flux ratio of inner broad $H\alpha$ to intermediate broad $H\alpha$, $\sim 2.6 - 3$, it is clear that intermediate broad component of $H\alpha$ is distinct and clearly decomposed in the mean spectrum of PG 0052+251. Certainly, we also try to fit broad $H\beta$ by two broad gaussian functions. However, intermediate broad component of $H\beta$ is not reliable due to smaller measured line width and line luminosity than corresponding measured uncertainties for the expected intermediate component of $H\beta$, which is consistent with results shown in Figure 3. The results indicate the intermediate broad component of BLR probably exists and is seriously obscured (no intermediate broad component of $H\beta$) for PG 0052+251. Certainly, the intermediate broad component of $H\beta$ can not be detected perhaps due to low quality of spectra for PG 0052+251. Although there is no true value of flux ratio of intermediate broad component of $H\alpha$ to intermediate broad component of $H\beta$, it is not difficult to determine cut-off value of S/N (signal to noise) for future high quality of spectra. If we accept flux ratio of intermediate broad component of $H\alpha$ to intermediate broad component of $H\beta$ is about 6, S/N should be larger than 24.

Before the end of the subsection, we discuss properties of χ^2 for fitted results for $H\alpha$ and $H\beta$, in order to find more reliable evidence for the existence of the second gaussian component for $H\alpha$. Here χ^2 is value of summed

squared residuals for measured parameters divided by degree of freedom, which can be used as one good indicator to determine whether fitted results are acceptable. Here, we accept uncertainty for flux is about $\sim 10\%$. The values of χ^2 are 0.18, 0.06 and 0.08 for best fitted results by one gaussian functions and by two gaussian functions for $H\alpha$ and by gaussian functions for lines around $H\beta$ respectively. Then based on fitted results by one or two gaussian functions for $H\alpha$, F-test is performed: at 99% confidence level, calculated variance ratio of results by one gaussian function to results by two gaussian functions is 2.14 for $H\alpha$ in mean spectrum, which is much larger than F value 1.34. The results indicate two gaussian functions for $H\alpha$ is necessary. Due to the unreliable second gaussian component for $H\beta$ through least-squares minimization method, F-test is not performed for results of $H\beta$.

3.3. Properties of Observed Spectra

We consider observed spectra collected from Kaspi et al. (2000) in the subsection. Line parameters are measured through gaussian functions for all the 55 observed spectra with both $H\alpha$ and $H\beta$ for PG 0052+251, as what we have done above for balmer lines in the mean spectrum. Emission lines around $H\beta$ are measured once: only a single broad component is fitted for $H\beta$. Emission line $H\alpha$ is measured twice, 1): one broad gaussian function is fitted for $H\alpha$, 2): two broad gaussian functions are fitted for $H\alpha$, one broad component and the other intermediate broad component as shown in subsection above. When two gaussian functions are applied to fit $H\alpha$, broad component has similar line width as the one of broad $H\beta$ (with a permitted scatter of 0.1dex) and line width ratio of the corresponding two functions (broad to intermediate broad) is fixed to 2.16 ($\sim \frac{2370\text{km/s}}{1100\text{km/s}}$, based on the measured line widths of two components of $H\alpha$ in the mean spectrum).

After the measurements of line parameters, we can find if one gaussian function is applied to fit $H\alpha$, line width ratio of total broad $H\beta$ to total broad $H\alpha$ is about 1.4 ± 0.1 , which is much larger than the mean value ~ 1.1 for quasars shown in Greene & Ho (2005) and larger than the theoretical value $\sim 1.06 - 1.1$ in Korista & Goad (2004). Furthermore, if one gaussian function is applied to fit $H\alpha$, flux ratio of total broad $H\alpha$ to total broad $H\beta$ (Balmer decrement) is about 6.8, which is a larger and unreasonable value for blue quasar PG 0052+251 (mean value from composite spectra of quasar is about 3.56 in Vanden Berk et al. 2001). However, if two gaussian functions are applied to fit $H\alpha$, flux ratio of inner broad $H\alpha$ to inner broad $H\beta$ (observed total broad $H\beta$ only includes the inner broad $H\beta$, intermediate broad $H\beta$ is seriously obscured) is about 3.61 which is consistent with the value from composite spectra of quasars (Vanden Berk et al. 2001), and line width ratio is about $\sigma_{H\alpha}/\sigma_{H\beta} \sim 0.94$ (here $H\alpha$ is the one without intermediate broad $H\alpha$), which is consistent with the result shown in Greene & Ho (2005) and in Korista & Goad (2004), $H\beta$ is slightly larger than $H\alpha$ ($\sigma_{H\alpha}/\sigma_{H\beta} \sim 0.91$). Certainly, we should note that there are some cases that intermediate broad $H\alpha$ is too weak to be detected in observed spectra, as one example shown in Figure 4, which

is probably due to the observed spectra with lower resolution. It is clear that total observed broad H α separated into two components (one inner broad component and one intermediate broad component) should be more reasonable for blue quasar PG 0052+251.

3.4. CCF Results

Finally, we consider results from cross correlation function (CCF function) applied to measure size of BLR of PG 0052 +251, which can be determined by time lag between variations of continuum emission and variations of broad lines emission. Here the variations of broad emission lines have four components, variations of observed broad H β (inner broad H β), variations of observed total broad H α , variations of inner broad H α (coming from inner BLR) and variations of intermediate broad H α (coming from intermediate BLR). Here the used flux densities of total broad H α , H β and continuum emission are collected from Kaspi et al. (2000). And then, according to the measured flux ratio of broad H α to intermediate broad H α of each observed spectrum, the CORRECTED flux density of total broad H α for each observed spectrum can be separated into two values for inner broad component and for intermediate broad component of H α . Thus, effects from different instruments in different configurations can be totally ignored (van Groningen & Wanders 1992). In other words, the following used flux densities of broad line components are reliable.

Here, common interpolated cross-correlation function (ICCF) (Gaskell & Sparke 1986; Gaskell & Peterson 1987; Peterson 1993) is applied to quantify time lag between continuum emission and broad lines emission. We do not consider z-transfer discrete correlation function (ZDCF, Alexander 1997; Edelson & Krolik 1988; White & Peterson 1994) any more, because results from ZDCF are excellent agreement with results from ICCF (Peterson et al. 1991, 1992, 2004; Kaspi et al. 2000; Bentz et al. 2010). Figure 5 shows the final results based on the four broad components of H α and H β , including measured sizes of BLR and corresponding uncertainties determined by bootstrap method (Press et al. 1992; Peterson et al. 1998). Measured sizes of BLR based on variations of different broad components are listed in Table 2. The size of inner BLR is about 110 light-days based on inner broad H α (or observed broad H β) and the size of intermediate BLR based on intermediate broad H α is about 700 light-days. Furthermore, the measured sizes based on observed total broad H α and H β are consistent with the reported values in Kaspi et al. (2000, 2005) and in Peterson et al. (2004).

The clear size of intermediate broad component of H α through CCF results indicate the intermediate BLR for H α PG0052 can be mathematically determined. Based on the result, we try to discuss some unique characters based on intermediate BLR.

3.5. Intermediate BLR

Before to give some clear and further conclusion for mapped AGN PG0052. We discuss effects of intermediate BLR on virial BH masses as follows.

There are two parameters used for virial BH masses in Equation (1), line width and size of BLR. The two parameters are based on observational information. If

intermediate broad component was accepted for H α of PG0052, we will find that virial BH mass estimated from properties of total observed broad H α (one inner broad component plus one intermediate broad component) should be some different from BH mass estimated from inner (or intermediate) broad component, and that estimated virial BH mass based on only inner (or intermediate) broad component of H α should be more accurate than virial BH mass based on total observed broad H α . Under the assumption of intermediate BLR accepted for H α of PG0052, we would find that

$$\begin{aligned}\sigma_{H\alpha}^2 &\simeq f_1 \times \sigma_{H\alpha_1}^2 + f_2 \times \sigma_{H\alpha_2}^2 \\ R_{BLR}^{H\alpha} &\simeq f_1 \times R_{BLR}^{H\alpha_1} + f_2 \times R_{BLR}^{H\alpha_2}\end{aligned}\quad (4)$$

where $\sigma_{H\alpha_1}$ ($R_{BLR}^{H\alpha_1}$) and $\sigma_{H\alpha_2}$ ($R_{BLR}^{H\alpha_2}$) mean measured line widths (sizes of BLR) based on inner broad component and intermediate broad component of H α , f_1 and f_2 represent parameter of flux weight: flux ratio of inner (intermediate) broad component to total observed broad H α ($f_1 + f_2 = 1$). One simple but clear method to prove the equation above can be found in Appendix.

It is very interesting that for PG0052 (only inner broad component for H β but inner broad plus intermediate broad component for H α), virial BH masses based on total observed broad H α should depends on properties of inner and intermediate component of H α

$$\begin{aligned}M_{BH} &\propto \sigma_{H\alpha}^2 \times R_{BLR}^{H\alpha} \\ &\propto (f_1^2 + f_2^2)(\sigma_{H\alpha_1}^2 \times R_{BLR}^{H\alpha_1}) \\ &\quad + f_1 f_2 (\sigma_{H\alpha_1}^2 \times R_{BLR}^{H\alpha_2} + \sigma_{H\alpha_2}^2 \times R_{BLR}^{H\alpha_1})\end{aligned}\quad (5)$$

In the equation above, relation $\sigma_{H\alpha_1}^2 \times R_{BLR}^{H\alpha_1} \simeq \sigma_{H\alpha_2}^2 \times R_{BLR}^{H\alpha_2}$ is accepted (BH mass estimated through properties of inner broad H α should be similar as mass through properties of intermediate broad H α). Then we can compare BH masses based on observed total broad H β (inner broad component for H β) and virial BH masses based on observed total broad H α

$$\frac{\sigma_{H\alpha}^2 \times R_{BLR}^{H\alpha}}{\sigma_{H\beta}^2 \times R_{BLR}^{H\beta}} \simeq (f_1^2 + f_2^2) + f_1 f_2 \left(\frac{R_{BLR}^{H\alpha_1}}{R_{BLR}^{H\alpha_2}} + \frac{R_{BLR}^{H\alpha_2}}{R_{BLR}^{H\alpha_1}} \right) \quad (6)$$

In the equation above, the relation $\sigma_{H\beta}^2 \times R_{BLR}^{H\beta} \simeq \sigma_{H\alpha_1}^2 \times R_{BLR}^{H\alpha_1} \simeq \sigma_{H\alpha_2}^2 \times R_{BLR}^{H\alpha_2}$ is accepted (BH masses estimated through inner broad H β (i.e., observed broad H β) should be similar as mass estimated on inner broad H α). Thus, intermediate broad component of H α for PG0052 should lead to some different virial BH mass through total observed broad H β (only one inner broad component in observed spectrum) and total observed broad H α (one inner broad component plus one intermediate broad component), and lead to the result that PG0052 should be one outlier in the plane of $\sigma_{H\beta}^2/\sigma_{H\alpha}^2$ vs $R_{BLR}^{H\alpha}/R_{BLR}^{H\beta}$.

Now let us check results of Equation (6) for PG 0052+251. Flux ratio of inner broad H α to intermediate broad H α (total observed broad H α minus intermediate broad H α) is about 2.5 to 3 (2.5 from mean spectrum, and 3 for observed spectra), size ratio of intermediate BLR (for intermediate broad H α) to inner BLR (for inner broad H α) is about 6-7. Then the ratio of $\sigma_{H\alpha}^2 \times R_{BLR}^{H\alpha}$

to $\sigma_{H\beta}^2 \times R_{BLR}^{H\beta}$ should be about 2 based on Equation (6), which is well agree with position of PG 0052+251 in the Figure 1. In the Figure 1, the area marked by dotted lines shows the accepted range for ratio of $\sigma_{H\alpha}^2 \times R_{BLR}^{H\alpha}$ to $\sigma_{H\beta}^2 \times R_{BLR}^{H\beta}$ under the size ratio of $R_{BLR}^{H\alpha 2}/R_{BLR}^{H\alpha 1} \sim 6-7$, based on Equation (6). Furthermore, it is simple to check and confirm the correlations shown in Equation (4). The results indicate outlier PG 0052+251 in Figure 1 can be perfectly explained by properties of intermediate broad component of $H\alpha$, which further indicate the intermediate broad component (or intermediate BLR) is reasonable.

Before the end of the subsection, we can compare our measured size of intermediate BLR with reported results about size of intermediate BLR in literature. Zhu et al. (2009) have found one correlation between size of intermediate BLR and central BH masses (Figure 7 in Zhu et al. 2009). If we accept $M_{BH} \sim (3.69 \pm 0.76) \times 10^8 M_\odot$ for PG 0052+251 (Peterson et al. 2004), then estimated size of intermediate BLR based on correlation shown in Zhu et al. (2009) is consistent with our measured value of $\sim 10^{18}$ cm, which provide further reliable evidence for intermediate BLR.

3.6. Extended Part of Inner BLR?

One question for existence of intermediate BLR is whether the component is only probable extended part of inner BLR, but not one isolated region. We answer the question as follows. Based on the results above, there are large distance between inner BLR and intermediate BLR, about 600 light-days. If the probable intermediate BLR is just the extended part of inner BLR, the BLR of PG0052 should have a much extended size. So large extended size of BLR should smooth variations of observed broad emission lines, in other words, there should be no apparent variations of broad emission lines. We check the effects of extended size of BLR on variations by following mathematical procedure.

Before proceeding further, we accept the assumptions listed in Peterson (1993) for reverberation mapping technique, 1): continuum emission is from one central source which is much smaller than BLR, 2): both continuum emission and line emission are freely and isotopically propagating in central volume, 3): line emissions are in rapid response to ionizing continuum. Furthermore, we accept that line intensity from one region simply depends on number density of the region, $I \propto N(r)$ (some detailed discussion for emission lines of AGN can be found in Netzer 1990; Osterbroock & Ferland 2006). Moreover, we simply accept that BLR is spherical shell (center of the sphere at position of central black hole) with depth about 600 light-days (inner layer radius is about 90 light-days, outer layer is about 700 light-days). Then based on the geometrical structure, responded light curve of emission line based on input light curve of continuum emission can be created, as what we have done for 3C390.3 (Zhang 2011). The spherical shell (BLR) is firstly divided into M layers. As long as M is large enough, the effects of depth of each layer can be totally ignored. The line intensity from each layer (with radius r) can be determined by

$$I(r) \propto N(r) \propto 1/r^p \quad (7)$$

In order to find more clear effects of extended size of

BLR, $p \sim 0$ is accepted. If p is much large, the outer part of BLR should have few contributions to line emission. Thus, we select $p = 0$, there are similar flux strength from clouds in inner part of BLR and from clouds in outer part of BLR, which will show more clear effects of extended size of BLR on observed light curve of broad line. Once one layer meets the ionizing photos from central source, the line intensity of the layer is changed immediately as,

$$I_i(t) \propto I_i(t-1) \times \frac{con_i(t)}{con_i(t-1)} \quad (8)$$

where t is the date, I_i and con_i mean line intensity from i th layer and arriving continuum emission (discrete data series with time separation of 1 day) for the layer.

There is one point we should note that in our mathematical procedure, the most simplest spherical shell geometry is assumed for BLR. Actually the geometry is perhaps some different from true structure of BLR of PG 0052+251. As discussed in Gaskell (2009); Eracleous et al. (2009); Sluse et al. (2011); Bentz et al. (2010a) and reference therein, BLRs of AGN have a flattened distribution and that we always view them near pole-on, and BLR structures are very similar in most AGN. Although, the applied spherical shell geometry is oversimplified for PG 0052+251, results based on the simplified structure can still indicate true effects of extended size of BLR on observed light-curve of broad line. Different structures of BLR should lead to some different overall trend of observed light-curves of broad lines (such as one example shown in Zhang 2011), the large extended size of BLR still smooth observed light-curve of broad line. As one example to demonstrate effects of extended size of BLR, the oversimplified structure of BLR is significantly valid.

Due to the simple procedure above, responded light curve of $H\alpha$ based on light curve of continuum emission of PG0052 can be created and shown in Figure 6. It is clear that the responded light curve of $H\alpha$ is very smooth, if extended size of BLR is about 600 light-days, i.e., if calculated intermediate BLR of PG0052 is just extended part of inner BLR. Furthermore, we also show one tested light curve of $H\alpha$, if BLR has smaller extended size about 30 light-days. For the case with small extended size of BLR, some subtle features (arrows in the figure) shown in light curve of continuum emission can be reflected in light curve of emission line, however the features can not be found in created light curve of emission line for BLR with larger extended size. In the subsection, to clearly describe structures of BLR of PG0052 is not our objective. Thus, we do not shown further results any more. The results shown in Figure 6 clearly indicate that the intermediate BLR can not be treated as extended part of inner BLR for PG0052, otherwise, the observed light curve of $H\alpha$ should be much smooth.

4. DISCUSSIONS

After study of BLR of AGN for more than half one century, some information about geometrical structures of BLR has been mathematically determined by transfer function in the reverberation mapping technique through some special mathematical methods (such as Maximum Entropy Method, Narayan & Nityananda 1986; Peterson 1993; Peterson et al. 1994; Horne et al. 1991; Goad et al.

1993; Wanders & Horne 1994; Pijpers & Wanders 1994; Krolik 1994; Winge et al. 1995; Bentz et al. 2010a; Sluse et al. 2011). Certainly, besides the results through mathematical methods, there are some statistical results about structures of BLR of AGN (some reviews can be found in Gaskell 2009; Eracleous et al. 2009; Down et al. 2010), based on properties of observed broad broad emission lines, such as the proposed model that one much broader component for wing of broad emission line and one intermediate broad component for core of broad emission line (Zhu et al. 2009; Hu et al. 2008; Sulentic et al. 2000; Brotherton et al. 1994; Brotherton 1996; Mason et al. 1996; Bon et al. 2009; Popovic 2007). However, evidence is not so sufficient to confirm intermediate BLR of AGN. In this paper, besides the fitted results for broad Balmer emission lines, properties of line cores from PCA technique and the measured size of expected intermediate BLR are further confirmed evidence for intermediate BLR of PG 0052+251: besides one common inner component of BLR (inner BLR) with size about 100 light days, there is one other seriously obscured intermediate component of BLR (intermediate BLR) with size about 700 light days.

Before proceeding further, we first simply consider one question what geometry is envisioned for intermediate BLR, where it suffers much more reddening than component giving rise to the inner BLR for PG 0052+251? Actually, it is not difficult to answer the question. Obscuration for intermediate BLR is not due to dust torus, but due to high density dust clouds (radial moving or not) between line-of-sight and intermediate BLR. The dust clouds have apparent effects on intermediate BLR, but no effects on inner BLR, due to small size of the clouds. The dust clouds can be confirmed by the special kind of AGN, AGN with their types changing between type 1 and type 2, such as Mrk1018 (Cohen et al. 1986; Goodrich 1990), NGC 7603 (Tohline & Osterbrock 1976), NGC 2622 and Mrk 609 (Goodrich 1990) etc.. The large distance between inner BLR and intermediate BLR for PG0052 (about 600light-days) ensures enough space for the dust clouds.

Furthermore, we consider the vitalization assumption (Gaskell 1988; Wandel et al. 1999; Peterson & Wandel 1999) for intermediate BLR. As discussed in Brotherton et al. (1994) through simple photoionization model, properties of inner BLR and intermediate BLR are consistent with virialization assumption

$$V_1^2 \times R_{\text{BLR},1} \sim V_2^2 \times R_{\text{BLR},2} \quad (9)$$

R_{BLR} means size of BLR (distance between BLR and central black hole) and V represents the rotating velocity of broad emission line clouds in corresponding BLR (commonly, line width of broad emission lines, the second moment). For PG 0052+251, the sizes of two components of BLR and line widths of inner broad and intermediate broad components have been measured above,

$$\left(\frac{\sigma_{\text{H}\alpha_1}}{\sigma_{\text{H}\alpha_2}} \right)^{2.0} = 4.7 \pm 0.4 \simeq \frac{R_{\text{BLR}}^{\text{H}\alpha_2}}{R_{\text{BLR}}^{\text{H}\alpha_1}} = 6 \pm 1.5 \quad (10)$$

Here, the mean value $(\sigma_{\text{H}\alpha_1}/\sigma_{\text{H}\alpha_2})$ is calculated by the measured line parameters for all observed spectra of PG 0052+251, which is consistent with the one from mean spectrum of PG 0052+251. The value of $R_{\text{BLR}}^{\text{H}\alpha_2}/R_{\text{BLR}}^{\text{H}\alpha_1}$ is

calculated by the measured sizes of BLR listed in Table 2. It is clear that the result is consistent with what we expect under the virialization method for BLR.

Certainly, some effects on measured line parameters of mapped AGN should be discussed. As discussed in Kaspi et al. (2000), the variable Fe II lines could alter line parameter measurements. However, Among the listed PG quasars in Table 1, PG 0052 and PG 0026 are the only two objects without apparent optical FeII lines, the other 5 PG quasars have strong and apparent FeII emission lines. However, only PG 0052 is one outlier in Figure 1. Thus, effects of FeII on measured line parameters can be totally ignored. Another question we should discuss is size of BLR could change, such as simple discussion in Kaspi et al. (2000) and detailed study and discussions for well-known mapped AGN NGC5548 (Bentz et al. 2006, 2007; Denney et al. 2010; Peterson et al. 2004; Wanders & Peterson 1996). However, we can find decreasing line width with increasing size of BLR, consistent with expected results under virialization assumption. Thus, effects of size of BLR changing could not explain the outliers in Figure 1.

Before the end of the section, we should note that it should be interesting to find candidates for AGN with intermediate BLR by the outliers in the plane of $R_{\text{BLR}}^{\text{H}\alpha}/R_{\text{BLR}}^{\text{H}\beta}$ vs $\sigma_{\text{H}\beta}^2/\sigma_{\text{H}\alpha}^2$, especially for objects with much larger values of $(\sigma_{\text{H}\alpha}^2 \times R_{\text{BLR}}^{\text{H}\alpha})/(\sigma_{\text{H}\beta}^2 \times R_{\text{BLR}}^{\text{H}\beta})$. Thus, we will expect that mapped object NGC 4253 should be strong candidate with intermediate BLR.

Finally, a simple summary is as follows. We first check properties of mapped AGN collected from literature in plane of $\sigma_{\text{H}\beta}^2/\sigma_{\text{H}\alpha}^2$ vs $R_{\text{BLR}}^{\text{H}\alpha}/R_{\text{BLR}}^{\text{H}\beta}$. Commonly, virial BH masses based on properties of observed broad H α and H β should be coincident. However, among the mapped objects with measured sizes of BLR and line widths (second moment) based on long-period observed broad H α and H β , PG0052 and NGC4253 are two apparent outliers in the plane of $\sigma_{\text{H}\beta}^2/\sigma_{\text{H}\alpha}^2$ vs $R_{\text{BLR}}^{\text{H}\alpha}/R_{\text{BLR}}^{\text{H}\beta}$, which indicate BLRs of PG0052 and NGC4253 have some special characters. Then based on 55 public spectra of PG0052 (Kaspi et al. 2000), the BLR of PG0052 is been carefully studied in detail. We find that line width ratio of total observed broad H α to total observed broad H β is ~ 0.7 , which is much smaller than theoretical/observational value of ~ 0.9 found by Korista & Goad (2004) and in Greene & Ho (2005). Furthermore, the flux ratio of total broad H α to total broad H β is about 6.8 (Balmer Decrement), which is not one reasonable value (mean value of 3.56 in Vanden Berk et al. 2001) for BLUE quasar PG 0052+251. Moreover, properties of line cores based on PCA technique indicate there is one inner broad component and one seriously obscured intermediate broad component in BLR. If the seriously obscured intermediate BLR was accepted, properties of PG0052 in the plane of $\sigma_{\text{H}\beta}^2/\sigma_{\text{H}\alpha}^2$ vs $R_{\text{BLR}}^{\text{H}\alpha}/R_{\text{BLR}}^{\text{H}\beta}$ could be well reproduced, which indicates that the intermediate BLR actually is well appropriate to mapped quasar PG 0052+251. Finally, the large distance between inner component of BLR and intermediate component of BLR based on CCF results (about 600light-days) indicates the intermediate

component is not extended part of inner component of BLR.

ACKNOWLEDGEMENTS

We gratefully acknowledge the anonymous referee for giving us constructive comments and suggestions to greatly improve our paper. ZXG gratefully acknowledges the support from NSFC-11003034, and gratefully thanks

Dr. Kaspi S. to provide us the available observed spectra of PG 0052 (<http://wise-obs.tau.ac.il/~shai/PG/>), and gratefully thanks AGNWATCH Project, and gratefully thanks Prof. Wang J.-M. for the discussions and constructive suggestions for the manuscript. This research has made use of NASA/IPAC Extragalactic Database (NED) which is operated by the Jet Propulsion Laboratory, California Institute of Technology, under contract with the National Aeronautics and Space Administration,

APPENDIX

TO PROVE EQUATION (4)

Based on definition of second moment (Peterson et al. 2004)

$$\sigma^2 = \frac{\int \lambda^2 \times P_\lambda d\lambda}{\int P_\lambda d\lambda} - \left(\frac{\int \lambda P_\lambda d\lambda}{\int P_\lambda d\lambda} \right)^2 = \frac{\int \lambda^2 \times P_\lambda d\lambda}{\int P_\lambda d\lambda} - \lambda_0^2 \quad (\text{A1})$$

where function P represents line profile, and λ represents wavelength. For broad $\text{H}\alpha$ of PG0052 which includes two components of $\text{H}\alpha_1$ (inner broad component) and $\text{H}\alpha_2$ (intermediate broad component), we can find the correlation between line width of total broad $\text{H}\alpha$ ($\sigma_{\text{H}\alpha}$) and line widths of the two components of $\text{H}\alpha$ ($\sigma_{\text{H}\alpha_1}$ and $\sigma_{\text{H}\alpha_2}$)

$$\begin{aligned} \sigma_{\text{H}\alpha}^2 &= f_1 \times \sigma_{\text{H}\alpha_1}^2 + f_2 \times \sigma_{\text{H}\alpha_2}^2 + f_1 \times \lambda_0^2(\text{H}\alpha_1) \\ &\quad + f_2 \times \lambda_0^2(\text{H}\alpha_2) - [f_1 \times \lambda_0(\text{H}\alpha_1) + f_2 \times \lambda_0(\text{H}\alpha_2)]^2 \\ &= f_1 \times \sigma_{\text{H}\alpha_1}^2 + f_2 \times \sigma_{\text{H}\alpha_2}^2 + G[\lambda_0(\text{H}\alpha_1), \lambda_0(\text{H}\alpha_2)] \end{aligned} \quad (\text{A2})$$

where f_1 and f_2 are flux ratios of separated broad components of $\text{H}\alpha$ to total broad $\text{H}\alpha$, i.e., $f_1 = \int P_{\lambda,1} d\lambda / \int P_\lambda d\lambda$, $f_2 = \int P_{\lambda,2} d\lambda / \int P_\lambda d\lambda$ and $f_1 + f_2 = 1$. $\lambda_0(\text{H}\alpha_1)$ and $\lambda_0(\text{H}\alpha_2)$ are the first moments (center wavelengths) of the two components of broad $\text{H}\alpha$. It is clear that if inner component and intermediate broad component have not so much large different center wavelengths ($\lambda_0(\text{H}\alpha_1) \simeq \lambda_0(\text{H}\alpha_2)$), the equation $\sigma_{\text{H}\alpha}^2 \simeq f_1 \times \sigma_{\text{H}\alpha_1}^2 + f_2 \times \sigma_{\text{H}\alpha_2}^2$ can be safely accepted.

To mathematically prove equation $R_{\text{BLR}}^{\text{H}\alpha} \simeq f_1 \times R_{\text{BLR}}^{\text{H}\alpha_1} + f_2 \times R_{\text{BLR}}^{\text{H}\alpha_2}$ should be very difficult. Here, we prove the equation by following Monte-Carlo method, based on completely HOMOGENEOUS light-curves of continuum emission ($C(t)$) and broad line emission ($L(t)$) of well-known reverberation-mapped AGN NGC5548 (Peterson et al. 2002) collected from AGNWATCH project (<http://www.astronomy.ohio-state.edu/~agnwatch/>). Light curves of inner and intermediate broad $\text{H}\alpha$ are created through bootstrap method (one common used monte-carlo method to create a mock population from a given sample of data) applied to light curve of broad line $\text{H}\beta$ of NGC5548. Observed light curve of NGC5548 including N data points can be described as $[t_i, \text{flux}_i]$, where index $i = 1, 2, \dots, N$ means the i th data points in light curve, t and flux represent the observational date and corresponding flux density of emission line. In order to simply our mathematic procedure, the date t_i is re-created as isolated integral values with step of 1 day based on observed data series of NGC5548. Then mock light curves of inner and intermediate broad components of $\text{H}\alpha$ can be created by the following two steps. On the first step, through the bootstrap method, a new sample of index from 1 to N , $k = 1, \dots, N$, is created. Certainly, there are some same values in sample of k . On the second step, mock light curve of inner broad $\text{H}\alpha$ is created by $[t_i, \text{flux}_k]$, mock light curve of intermediate broad $\text{H}\alpha$ is created by $[t_i + \Delta, \text{flux}_k \times f_{\text{sca}}]$, where $\Delta \in [2, 160]$ days are integral values and represent distances between inner BLR and intermediate BLR, and $f_{\text{sca}} \in [0.2, 5]$ represents flux density ratio of intermediate broad $\text{H}\alpha$ to inner broad $\text{H}\alpha$. Values of f_{sca} ensure both the two broad components of $\text{H}\alpha$ are apparent. Parameter Δ ensures that there is longer distance between intermediate BLR and central black hole than the distance between inner BLR and central black hole. Then the two steps above are repeated, until there are enough mock light curves. Furthermore, based on the bootstrap method, effects of simply different geometrical structures of inner and intermediate components of BLR have been simply included (simple results about effects of geometric structures of BLR on measured size of BLR can be found in Zhu et al. 2009). Based on the created mock light curves (date and flux density: $[t_{i,\text{inner}}, \text{flux}_{k,\text{inner}}]$ and $[t_{i,\text{inter}}, \text{flux}_{k,\text{inter}}]$) of inner and intermediate component, it is easy to create the mock light curves ($[t_{i,\text{tot}}, \text{flux}_{k,\text{tot}}]$) of total broad line (inner component plus intermediate component) by

$$\begin{aligned} t_{i,\text{tot}} &= t_{i,\text{inter}} \quad \text{if} \quad t_{i,\text{inter}} = t_{i,\text{inner}} \\ t_{i,\text{tot}} &\text{ rejected} \quad \text{if} \quad t_{i,\text{inter}} \neq t_{i,\text{inner}} \\ \text{flux}_{k,\text{tot}} &= \text{flux}_{k,\text{inner}} + \text{flux}_{k,\text{tot}} \quad \text{if} \quad t_{i,\text{inter}} = t_{i,\text{inner}} \\ \text{flux}_{k,\text{tot}} &\text{ rejected} \quad \text{if} \quad t_{i,\text{inter}} \neq t_{i,\text{inner}} \end{aligned} \quad (\text{A3})$$

Then values of $R_{\text{BLR}}^{\text{H}\alpha}$, $R_{\text{BLR}}^{\text{H}\alpha_1}$ and $R_{\text{BLR}}^{\text{H}\alpha_2}$ can be determined by CCF function. Here we notice that only CCF result with one apparent peak is accepted. Figure 7 shows the correlation (coefficient 0.97 with significance of deviation

TABLE 1
PARAMETERS FOR THE 16 MAPPED AGN

name	$\sigma_{H\alpha}$ km/s	$R_{BLR}^{H\alpha}$ light-days	$\sigma_{H\beta}$ km/s	$R_{BLR}^{H\beta}$ light-days	Public
PG0026+129	1961±135	98.1 ^{+28.3} _{-25.5}	1773±285	111.0 ^{+24.1} _{-28.3}	Kaspi
PG0052+251	1913±85	163.7 ^{+58.5} _{-38.3}	1783±86	89.8 ^{+24.5} _{-24.1}	Kaspi
PG0804+761	2046±138	183.6 ^{+15.3} _{-13.3}	1971±105	146.9 ^{+18.8} _{-18.9}	Kaspi
NGC4151	2422±79	3.2 ^{+1.9} _{-1.7}	1914±42	3.1±1.3	AGNWATCH
PG1411+442	2437±196	94.7 ^{+36.0} _{-31.5}	1607±169	124.3 ^{+61.0} _{-61.7}	Kaspi
PG1426+015	4254±290	75.5 ^{+30.5} _{-32.5}	3442±308	95.0 ^{+29.9} _{-37.1}	Kaspi
PG1617+175	2483±160	94.2 ^{+19.1} _{-25.2}	2626±211	71.5 ^{+29.6} _{-33.7}	Kaspi
PG2130+099	1421±80	198.4 ^{+32.6} _{-23.4}	1623±86	158.1 ^{+29.8} _{-18.7}	Kaspi
NGC7469	1164±68	4.7 ^{+1.6} _{-1.3}	1456±207	4.5 ^{+0.7} _{-0.8}	AGNWATCH
Mrk142	934±61	2.90 ^{+1.22} _{-0.92}	859±102	2.87 ^{+0.76} _{-0.87}	NO
SBS1116+583A	1218 ⁺¹⁴⁷ ₋₉₉	4.12 ^{+1.41} _{-0.98}	1528±184	2.38 ^{+0.64} _{-0.51}	NO
Arp151	937±34	8.01 ^{+1.09} _{-1.00}	1252±46	4.08 ^{+0.50} _{-0.69}	NO
Mrk1310	717±75	4.60 ^{+0.67} _{-0.62}	755±138	3.74 ^{+0.60} _{-0.62}	NO
NGC4253	726±35	25.50 ^{+0.66} _{-0.86}	516±218	6.24 ^{+1.65} _{-1.24}	NO
NGC4748	1035±74	7.61 ^{+3.01} _{-4.64}	657±91	5.63 ^{+1.64} _{-2.25}	NO
NGC6814	1082±52	9.51 ^{+1.91} _{-1.56}	1610±108	6.67 ^{+0.88} _{-0.90}	NO

Notice:— 'Kaspi' means public observed spectra can be found from website <http://wise-obs.tau.ac.il/~shai/PG/>.

'AGNWATCH' means public observed spectra can be found from the AGNWATCH project <http://www.astronomy.ohio-state.edu/~agnwatch/>.

'NO' means there are no public observed spectra, the listed parameters are collected from Bentz et al. (2010).

Size of BLR based on broad Balmer emission lines are the ones determined by the τ_{cent} , and line widths are the ones measured from rms spectra as discussed in Peterson et al. (2004).

We should note: listed values of parameters are values from more recent literature.

TABLE 2
PARAMETERS OF PG 0052+251

Line	σ Å	flux $10^{-16}\text{erg/s/cm}^2$	$R_{BLR}(p)$ light-days	$R_{BLR}(c)$ light-days	$R_{CCF}(max)$
H β (broad)	38.4	1426.3	109±25	111±15	0.76
H α (tot broad)	37.4	9612.5	191±24	214±19	0.72
H α (inner broad)	51.8	5067.9	110±20	116±16	0.68
H α (int broad)	24.1	1649.5*	703±45	678±40	0.38

Notice:— H α (tot broad) means observed total broad H α . H α (inner broad) means inner broad component of H α . H α (int broad) represents intermediate broad component of H α .

Second column gives the second moment of broad component in unit of Å shown in mean spectrum of PG 0052+251, third column shows measured mean flux density of broad component for 55 observed spectra of PG 0052+251, fourth column shows measured size of BLR through peak value of CCF results, fifth column shows the measured size of BLR through central value of CCF results, sixth column shows the maximum coefficient through CCF.

Corresponding error of measured size of BLR is determined through bootstrap method as shown in Figure 5

1649.5* means the mean value is not so reliable and probably lower than the internal value, due to much weak intermediate broad H α in some observed spectra.

from zero $P_{null} \sim 0$ for 664 simulated data points) between $R_{BLR}^{H\alpha}$ and $R_{BLR}^{H\alpha_1} \times f_1 + R_{BLR}^{H\alpha_2} \times f_2$ ($f_1 = 1/(1 + f_{sca})$ and $f_2 = f_{sca}/(1 + f_{sca})$). It is clear that the expected relation about size of BLR in Equation (4) can be commonly accepted. Furthermore, the results shown in Figure 7 indicate even there are two apparent two components in light curve of broad line, the CCF could be single-peaked not double-peaked appearance.

REFERENCES

- Alexander, T. 1997, in *Astronomical Time Series*, ed. D. Maoz, A. Sternberg, & E. M. Leibowitz (Dordrecht: Kluwer), 163
- Assef, R. J., Denney, K. D., Kochanek, C. S., Peterson, B. M., Kozłowski, S., et al., 2010, *astro-ph/1009.1145*
- Barth, A. J., Nguyen, M. L., Malkan, M. A., Filippenko, A. V., Li, W., et al., 2011, *ApJ*, 732, 121
- Bentz, M. C., Peterson, B. M., Pogge, R. W., Vestergaard, M., Onken, C. A., 2006, *ApJ*, 644, 133
- Bentz, M. C., Denney, K. D., Cackett, E. M., Dietrich, M., Fogel, J. K. J., et al., 2007, *ApJ*, 662, 205
- Bentz, M. C., Walsh, J. L., Barth, A. J., Baliber, N., Bennert, V. N., et al., 2009, *ApJ*, 705, 199
- Bentz, M. C., Horne, K., Barth, A. J., Bennert, V. N., Canalizo, G., et al., 2010a, *ApJ*, 720, L46
- Bentz, M. C., Walsh, J. L., Barth, A. J., Yoshii, Y., Woo, J.-H., et al., 2010, *ApJ*, 716, 993
- Blandford, R. D., & McKee, C. F., 1982, *ApJ*, 255, 419
- Bon, E., Popovic, L. C., Gavrilovic, N., Mura, G. L., Mediavilla, E., 2009, *MNRAS*, 400, 924
- Brotherton, M. S., Wills, B. J., Francis, P. J., Steidel, C. C., 1994, *ApJ*, 430, 495
- Brotherton, M. S., 1996, *ApJS*, 102, 1
- Cohen, R. D., Rudy, R. J., Puetter, R. C., Ake, T. B., Foltz, C. B., 1986, *ApJ*, 311, 135

- Collin, S., Kawaguchi, T., Peterson, B. M., Vestergaard, M., 2006, *A&A*, 456, 75
- Denney, K. D., Peterson, B. M., Dietrich, M., Vestergaard, M., Bentz, M. C., 2009a, *ApJ*, 692, 246
- Denney, K. D., Peterson, B. M., Pogge, R. W., Adair, A., Atlee, D. W., et al., 2009, *ApJ*, 704, L80
- Denney, K. D., Peterson, B. M., Pogge, R. W., Adair, A., Atlee, D. W., et al., 2010, *ApJ*, 721, 715
- Dimitrijevic, M. S., Popovic, L. C., Kovacevic, J., Dacic, M., Illic, D., 2007, *MNRAS*, 374, 1181
- Down, E. J., Rawlings, S., Sivia, D. S., Baker, J. C., 2010, *MNRAS*, 401, 633
- Edelson, R. A., & Krolik, J. H., 1988, *ApJ*, 333, 646
- Eracleous, M., Lewis, K. T., Flohic, H. M. L. G., 2009, *NewAR*, 53, 133
- Francis, P. J., Hewett, P. C., Foltz, C. B., Chaffee, F. H., 1992, *ApJ*, 398, 476
- Gaskell, C. M., & Sparke, L. S., 1986, *ApJ*, 305, 175
- Gaskell, C. M., & Peterson, B. M., 1987, *ApJS*, 65, 1
- Gaskell, C. M., 1988, *ApJ*, 325, 114
- Gaskell, C. M., 2009, *NewAR*, 53, 140
- Gaskell, C. M., 2010, submitted to *ApJ*, arXiv:1008.1057
- Goad, M. R., O'Brien, P. T., Gondhalekar, P. M., 1993, *MNRAS*, 263, 149
- Goodrich, R. W., 1990, *ApJ*, 355, 88
- Greene, J. E., & Ho, L. C., 2005, *ApJ*, 630, 122
- Greene, J. E., Hood, C. E., Barth, A. J., Bennert V. N., Bentz, M. C., et al., 2010, *ApJ*, 723, 409
- Horne, K., Welsh, W. F., Peterson, B. M., 1991, *ApJ*, 367, L5
- Hu, C., Wang, J.-M., Ho, L. C., Chen, Y.-M., Bian, W.-H., Xue, S.-J., 2008, *ApJ*, 683, L115
- Kaspi, S., Smith, P. S., Netzer, H., Maoz, D., Jannuzi, B. T., Givon, U., 2000, *ApJ*, 533, 631
- Kaspi, S., Maoz, D., Netzer, H., Peterson, B. M., Vestergaard, M., Jannuzi, B. T., 2005, *ApJ*, 629, 61
- Kelly, B. C., & Bechtold, J., 2007, *ApJS*, 168, 1
- Korista, K. T., & Goad, M. R., 2004, *ApJ*, 606, 749
- Krause, M., Burkert, A., Schartmann, M., 2011, *MNRAS*, 411, 550
- Krolik, J. H., 1994, *IAU Symposium No. 159: Multi-wavelength continuum emission of AGN*, p. 163 - 172
- Mason, K. O., Puchnarewicz, E. M., Jones, L. R., 1996, *MNRAS*, 283, 126
- McLure, R. J., & Dunlop, J. S. 2004, *MNRAS*, 352, 1390
- Narayan, R., & Nityananda, R., 1986, *ARA&A*, 24, 127
- Netzer, H. 1990, in *Active Galactic Nuclei*, ed. R. D. Blandford, H. Netzer, & L. Woltjer (Berlin: Springer), 137
- Netzer, H., & Marziani, P., 2010, *ApJ*, 724, 318
- Onken, C. A., Ferrarese, L., Merritt, D., Peterson, B. M., Pogge, R. W., Vestergaard, M., Wandel, A., 2004, *ApJ*, 615, 645
- Osterbrock, D. E., & Mathews, W. G., 1986, *ARA&A*, 24, 171
- Osterbrock, D. E., & Ferland, G. J., 2006, *Astrophysics of Gaseous Nebulae and Active Galactic Nuclei*, Second Edition, Mill Valley: University Science Books, ISBN 1-891389-34-3
- Pancoast, A., Brewer, B. J., Treu, T., 2011, *ApJ*, 730, 139
- Peterson, B. M., Balonek, T. J., Barker, E. S., Bechtold, J., Bertram, R., et al., 1991, *ApJ*, 368, 119
- Peterson, B. M., Alloin, D., Axon, D., Balonek, T. J., Bertram, R., et al., 1992, *ApJ*, 392, 470
- Peterson, B. M., 1993, *PASP*, 105, 247
- Peterson, B. M., Berlind, P., Bertram, R., Bochkarev, N. G., Bond, D., et al., 1994, *ApJ*, 425, 622
- Peterson, B. M., Wanders, I., Horne, K., Collier, S., 1998, *PASP*, 110, 660
- Peterson, B. M. & Wandel, A., 1999, *ApJ*, 521, L95
- Peterson, B. M., Berlind, P., Bertram, R., Bischoff, K., Bochkarev, N. G., et al., 2002, *ApJ*, 581, 197
- Peterson, B. M., Ferrarese, L., Gilbert, K. M., Kaspi, S., et al., 2004, *ApJ*, 613, 682
- Peterson, B. M. & Bentz, M. C., 2006, *NewAR*, 50, 796
- Peterson, B. M., 2010, *Co-Evolution of Central Black Holes and Galaxies*, Proceedings of the International Astronomical Union, IAU Symposium, Volume 267, p. 151-160
- Pijpers, F. P., & Wanders, I., 1994, *MNRAS*, 271, 183
- Popovic, L. C., 2007, *Exploring the Cosmic Frontier: Astrophysical Instruments for the 21st Century*. ESO Astrophysics Symposia, European Southern Observatory series. Edited by Andrei P. Lobanov, J. Anton Zensus, Catherine Cesarsky and Phillip J. Diamond. Series editor: Bruno Leibundgut, ESO. ISBN 978-3-540-39755-7. Published by Springer-Verlag, Berlin and Heidelberg, Germany, p.191
- Press, W. H., Teukolsky S. A., Vetterling W. T., Flannery B. P., 1992, 'Numerical Recipes in Fortran 77', Second Edition, published by the Press Syndicate of the University of Cambridge, ISBN 0-521-43064-X, P340
- Rafiee, A., & Hall, P. B., 2011, *ApJS*, 194, 42
- Shen, J., Vanden Berk, D. E., Schneider, D. P., Hall, P. B., 2008, *AJ*, 135, 928
- Sluse, D., Schmidt, R., Courbin, F., Hutsemekers, D., Meylan, G., Eigenbrod, A., Anguita, T., Agol, E., Wambsganss, J., 2011, *A&A*, 528, 100
- Sulentic, J. W., Marziani, P., Dultzin-Hacyan, D., 2000, *ARA&A*, 38, 521
- Sulentic, J. W., Repetto, P., Stirpe, G. M., Marziani, P., Dultzin-Hacyan, D., Calvani, M., 2006, *A&A*, 456, 929
- Sulentic, J. W., Bachev, R., Marziani, P., Negrete, C. A., Dultzin, D., 2007, *ApJ*, 666, 757
- Tohline, J. E., & Osterbrock, D. E., 1981, *ApJ*, 210, L117
- Vanden Berk, D. E., Richards, G. T., Bauer, A., Strauss, M. A., Schneider, D. P., et al., 2001, *AJ*, 122, 549
- van Groningen, E., & Wanders, I., 1992, *PASP*, 104, 700
- Vestergaard, M., 2002, *ApJ*, 571, 733
- Wandel, A., Peterson, B. M., & Malkan, M. A., 1999, *ApJ*, 526, 579
- Wanders, I., & Horne, K., 1994, *A&A*, 289, 7
- Wanders, I., & Peterson, B. M., 1996, *ApJ*, 466, 174
- Wang, T.-G., & Zhang, X.-G., 2003, *MNRAS*, 340, 793
- White, R. J., & Peterson, B. M., 1994, *PASP*, 106, 876
- Winge, C., Peterson, B. M., Horne, K., Pogge, R. W., Pastoriza, M., Storchi-Bergmann, T., 1995, *ApJ*, 445, 680
- Zhang, X.-G., 2011, *MNRAS* accepted, astro-ph/1107.0455
- Zhu, L., Zhang, S.-N., Tang, S., 2009, *ApJ*, 700, 1173

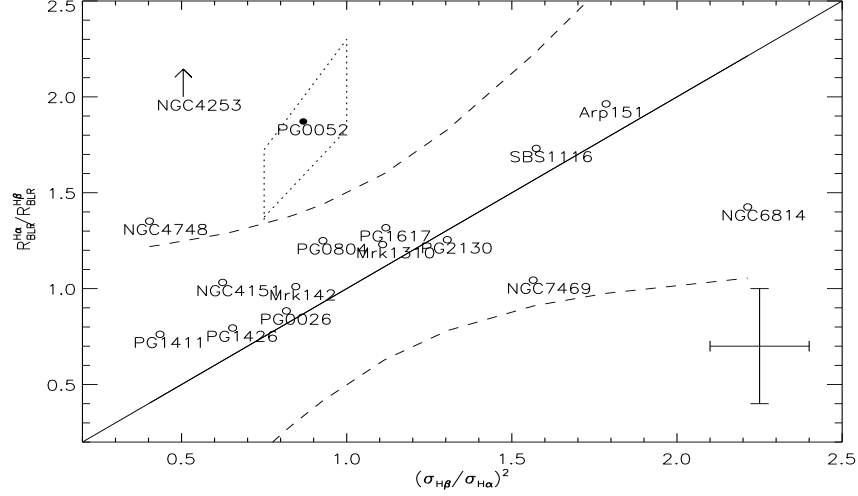


FIG. 1.— On the correlation between line width (second moment) ratio of $\sigma_{H\beta}^2/\sigma_{H\alpha}^2$ and size ratio of $R_{BLR}^{H\alpha}/R_{BLR}^{H\beta}$. Standard error bar for data points is shown in bottom right corner. Object PG 0052+251 is marked with solid circle. The area marked by dotted lines around PG 0052+251 represents the estimated area in the plane, if intermediate BLR was accepted for PG0052 (results from equation (6)). Solid line and dashed line represent the correlation $\sigma_{H\beta}^2/\sigma_{H\alpha}^2 = R_{BLR}^{H\alpha}/R_{BLR}^{H\beta}$ and its 99% confidence bands. For NGC4253, its true position $([0.51, 4.1])$ is much far away from the correlation. In order to clearly show the other objects, we use a upper arrow to represent that true position of NGC4253 should be much higher than the shown position $[0.51, 2]$.

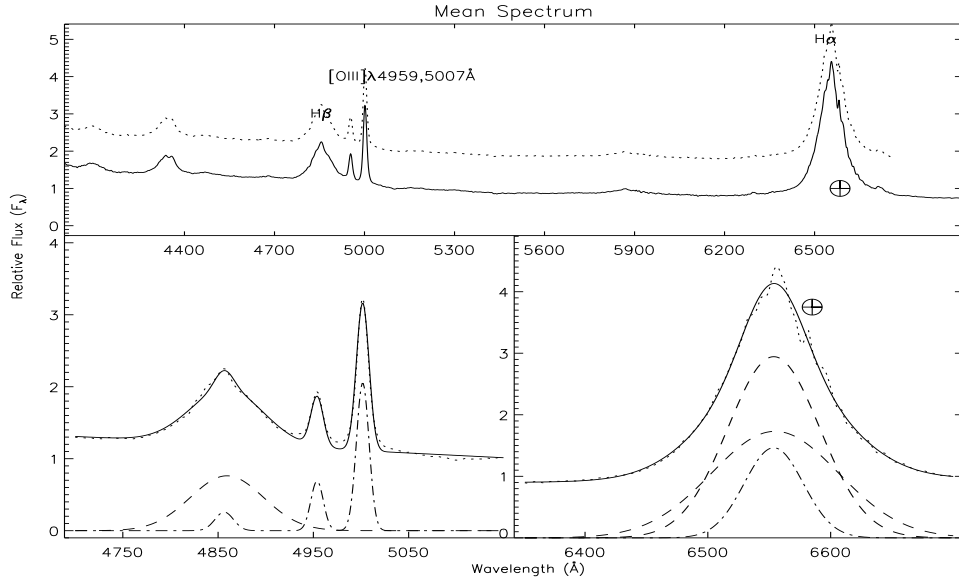


FIG. 2.— The mean spectrum of PG 0052+251, and best fitted results for emission lines around $H\alpha$ and $H\beta$. In top panel, solid line shows our mean spectrum created by PCA method ($flux(5100\text{\AA}) = 1$), dotted line shows the mean spectrum shown in Kaspi et al. (2000) ($flux(5100\text{\AA}) = 2$). In bottom-left panel, dotted line shows the mean spectrum around $H\beta$, thick solid line represents the best fitted results, dashed line represents broad component of $H\beta$ fitted by one broad gaussian function, dot-dashed line shows narrow components of $H\beta$ and $[OIII]\lambda 4959, 5007\text{\AA}$. In bottom-right panel, dotted line shows the mean spectrum around $H\alpha$, thick solid line represents the best fitted results. Thick dashed line shows broad component, if one broad gaussian function is applied to fit $H\alpha$. Thin dashed line shows the inner broad component, dot-dashed line shows the intermediate broad component, if two broad gaussian functions are applied to fit $H\alpha$. Symbols \oplus in the figure show positions of features of atmospheric A band near 7620\AA in observed frame.

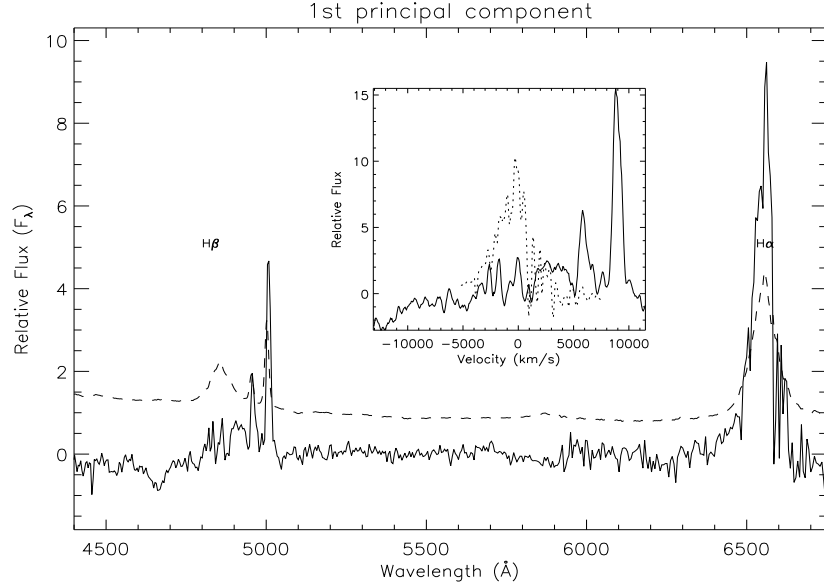


FIG. 3.— Properties of line cores. Solid line represents the first PCA component based on observed spectra with zero mean. Dashed line represents the mean spectrum based on observed spectra shown in Figure 2. Middle panel shows the comparison of line cores of $H\alpha$ and $H\beta$. In the panel, solid line represents line core of $H\beta$ with flux density scaled by 3, dotted line represents line core of $H\alpha$.

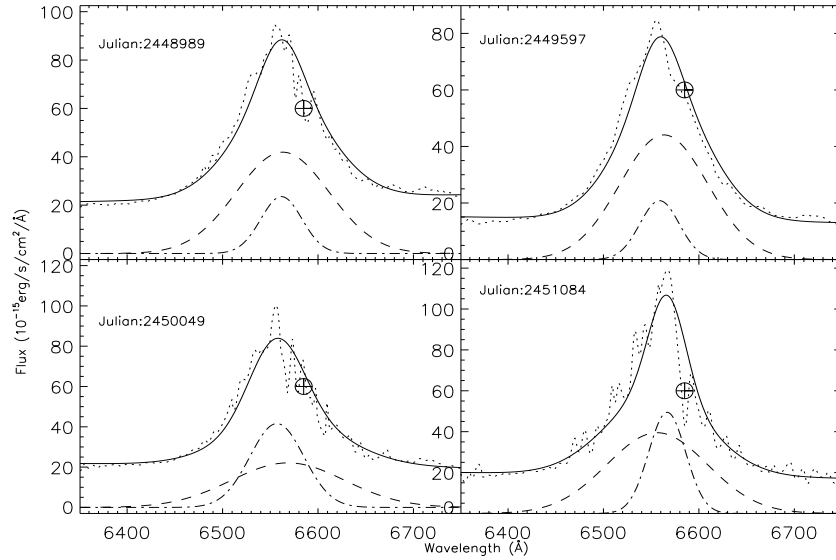


FIG. 4.— Best fitted results for observed $H\alpha$. In each panel, dotted line shows observed spectrum, thick solid line represents the best fitted results, dashed line represents inner broad component of $H\alpha$, dot-dashed line shows intermediate broad component of $H\alpha$. In the case of Julian:2449596 (top-right panel), there is no apparent intermediate broad component. Symbols \oplus in the figure show positions of features of atmospheric A band near 7620 Å in observed frame.

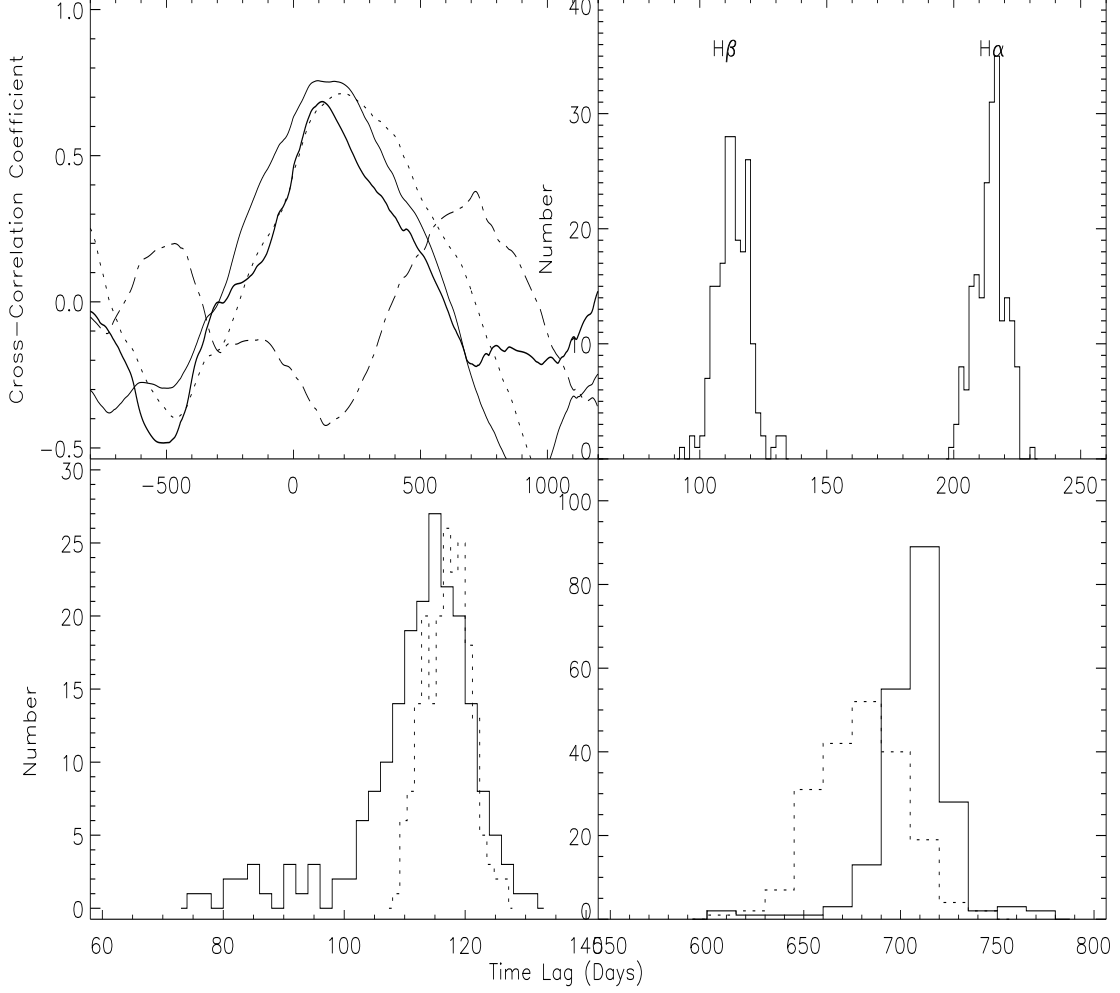


FIG. 5.— Top-left panel shows results about Cross-Correlation Function (CCF). Thin solid line represents the result for broad $H\beta$ ($CCF(H\beta, con_{5100\text{\AA}})$). Dotted line represents the result for total broad $H\alpha$ ($CCF(H\alpha_{tot}, con_{5100\text{\AA}})$). Thick solid line represents the result for inner broad $H\alpha$ ($CCF(H\alpha_{inner\ broad}, con_{5100\text{\AA}})$). Dot-dashed line shows the result for intermediate broad $H\alpha$ ($CCF(H\alpha_{int\ broad}, con_{5100\text{\AA}})$). Top right panel shows distributions of time-lags between total broad Balmer emission and AGN continuum emission through bootstrap method, in order to compare our results with the results shown in Kaspi et al. (2000) and in Peterson et al. (2004). Bottom-left panel shows distributions of time-lag between inner broad $H\alpha$ emission (after the subtraction of intermediate broad $H\alpha$) and AGN continuum emission through bootstrap method. Bottom-right panel shows distributions of time-lag between intermediate broad $H\alpha$ emission and AGN continuum emission through bootstrap method. In the two bottom panels, solid line represents the distributions for time-lag determined by peak values of CCF results, dotted line represents the distributions of time-lag determined by central values of CCF results.

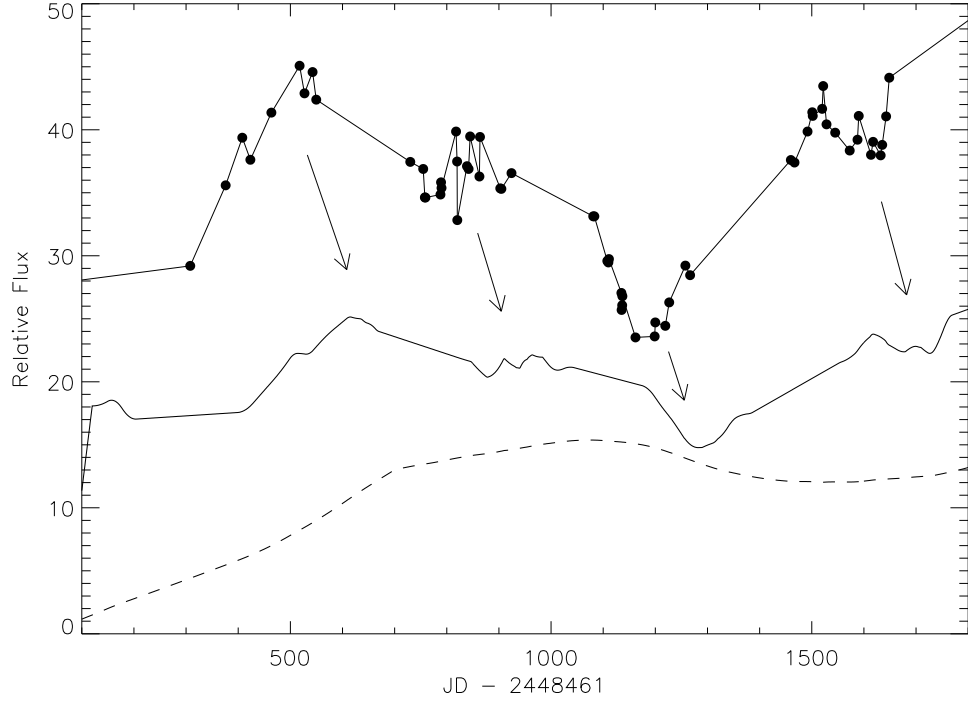


FIG. 6.— Effects of extended size of BLR on observed light curve of broad emission line. Solid line plus solid circle represents the observed light curve of continuum emission of PG0052, solid line represents the created light curve of emission line for the case that BLR with extended size about 30 light-days, dashed line represents the created light curve of emission line for the case that BLR with extended size about 600 light-days. The arrows show the positions of apparent features in light curve of continuum emission and in corresponding created light curve of emission line.

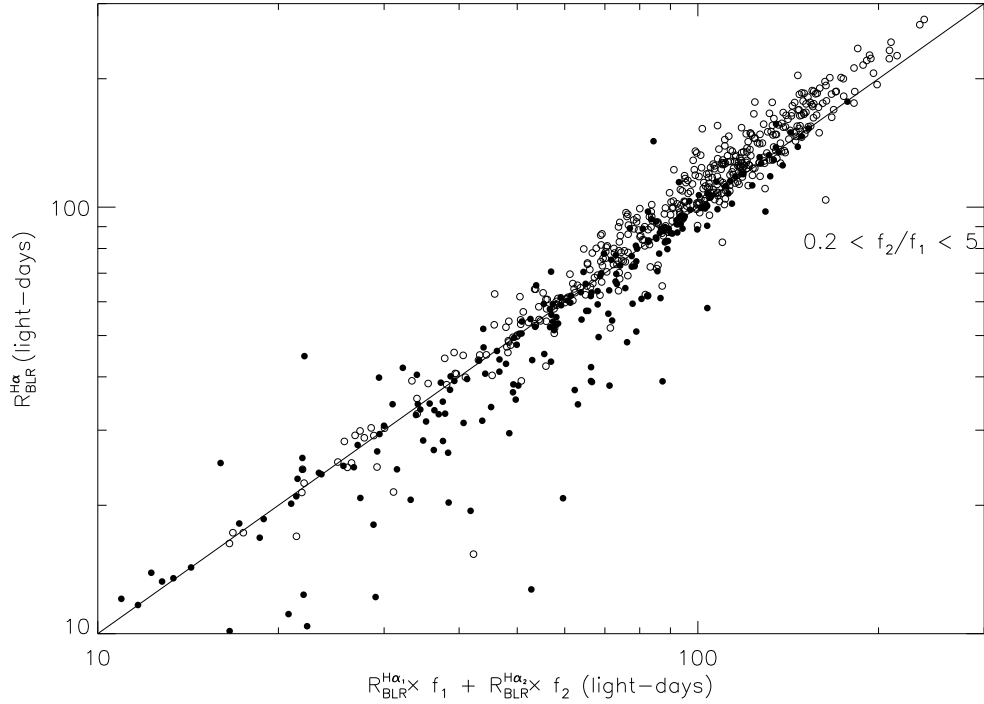


FIG. 7.— On the correlation between $R_{BLR}^{H\alpha}$ and $R_{BLR}^{H\alpha_1} \times f_1 + R_{BLR}^{H\alpha_2} \times f_2$ for total 664 simulated data points. Open circles represent 444 data points with $f_2/f_1 \geq 1$, and solid circles are for 220 data points with $f_2/f_1 \leq 1$. Solid line represents the relation $R_{BLR}^{H\alpha} = R_{BLR}^{H\alpha_1} \times f_1 + R_{BLR}^{H\alpha_2} \times f_2$.